

Identification and Visualization of the Underlying Independent Causes of the Diagnostic of Diabetic Retinopathy made by a Deep Learning Classifier

Jordi de la Torre^{a,*}, Aida Valls^a, Domenec Puig^a, Pedro Romero-Aroca^b

^a*Departament d'Enginyeria Informàtica i Matemàtiques.*

Escola Tècnica Superior d'Enginyeria.

Universitat Rovira i Virgili

Avinguda Paisos Catalans, 26. E-43007

Tarragona, Spain

^b*Ophthalmic Service. University Hospital Sant Joan de Reus*

Institut d'Investigació Sanitària Pere Virgili (IISPV)

Universitat Rovira i Virgili

Reus (Tarragona)

Avinguda de la Universitat, 1. E-43204

Reus, Spain

Abstract

Objectives: Deep learning models are parameterized functions with up to millions of parameters. Such a big parameter set makes impossible a direct interpretation of its internal logic. The goal of this paper is the proposal of a new method for compressing the internal representation of a deep learning classifier, obtaining a smaller set of disentangled feature components, more suitable for interpretation.

Methods: Deep learning models consist of two main parts: a feature extractor and a classifier. The statistical regularities present in the images are mapped by the feature extractor into a lower dimensional representation in the so-called feature space. The classifier combines such features obtaining a final classification. Such internal representations are much smaller than the input space dimensions but are still too big to be interpreted. Furthermore, typically feature dimensions are highly correlated. We propose a method based on

*Corresponding author

Email addresses: jordi.delatorre@gmail.com (Jordi de la Torre), aida.valls@urv.cat (Aida Valls), domenec.puig@urv.cat (Domenec Puig), romeropere@gmail.com (Pedro Romero-Aroca)

the use of an independent component analysis technique for compressing the feature-space.

Results: The method proposed has been used in a deep learning network constructed for the classification of diabetic retinopathy into 5 levels of severity. We find that its initial 64 dimensional internal feature representation can be compressed into a vector of only 3 dimensions, losing only 1.25% of performance in classification.

Conclusions: This methodology allows the generation of mathematically independent features from the highly redundant and correlated internal feature representation. Due to the linear nature of the calculated transformation, the new calculated components can be easily visualized in the input space for scoring pixel importance using any of the existing methods. We present some score maps on eye-fundus images using the pixel-wise explanation model.

Keywords: deep learning, classification, compression, diabetic retinopathy

2010 MSC: 68T10

1. Introduction

Diabetic Retinopathy (DR) is an associated disease derived from diabetes that is caused by the damage of the small blood vessels of the retina. Due to diabetes disease, some secondary effects appear, for instance retinal blood vessels can break down, leak or become blocked. These damages affect the transport of nutrients and oxygen to parts of the retina, causing impaired vision over time. Early detection allows its treatment and reduces substantially the negatives consequences associated with its development. Eye screening is used by physicians as a way for disease detection. Automatic classifiers can help in disease detection through the increase of the number of preventive analysis done over the diabetic population [1], [2].

Deep Learning (DL) [3], [4] is a subfield of Machine Learning that allows the automatic model construction of very effective image classifiers using a parametric model. These models are able to identify and extract the statistical

regularities present in data that are important for optimizing a defined loss function, with the final objective of mapping a high-multidimensional input into a smaller multi-dimensional output ($f: \mathbb{R}^n \mapsto \mathbb{R}^m, n \gg m$), enabling its categorization in small sets. They are parameterized models that are usually optimized using a stochastic gradient descent algorithm that minimizes a pre-defined loss function. These models are able to learn the statistical regularities present in data that allow the separation of the predefined classes [5], [6]. In DL, Convolutional Neural Networks (CNN) have proved to be very effective method for image classification, detection and segmentation.

DL models are organized in layers, being the inputs of each one a combination of the outputs of previous ones. The output layer is designed to be a linear combination of last layer feature space components. In this way we are forcing the model to disentangle the important features that, combined in a linear way, allow the achievement of a maximum possible classification score. These components (or others obtained as a linear combination of them, like with ICA analysis), are easy to analyze due to the linear nature of its relationship with the classification scores.

In this paper, we take an existing model based on CNN for classification of DR into 5 categories (presented by the authors in [7]) and now we propose a technique that allows the compression of the feature space and the identification of the mathematically independent elements of a DR DL classifier. The compression method proposed is based on keeping the level of classification quality obtained without the compression. Afterward, we show a pixel-wise score propagation method to visualize such independent component (IC) in the input space. The compression is done by calculating the minimum number of IC that are able to encode the maximum information about the particular classification. Identifying such components, we minimize the redundancy of feature space and we identify the components that share the minimum mutual information between each other. In that way, under the assumption that the feature extraction phase of the deep learning model has been able to disentangle completely the feature information, we are able to separate the independent elements causing

the disease.

Although we have made our study with one concrete DL model and visualization technique (from [7]), the proposed compression method is independent from the visualization method used and any other one could be also used for its interpretation. The novelty of the paper is based on the separation and visualization of the mathematically independent features that explain the DR classification. We use the assessment of experts clinicians for interpreting such IC.

The paper is structured as follows: in section 2 the current work on DL applied to DR is briefly introduced, then, the main works on interpretation of DL are presented. In section 3, we present the methods used in the paper and explain the compression technique based in ICA. Section 4 shows the results obtained. The discussion of such results is found in section 5. Finally in section 6 we present the final conclusions of our work.

2. Related Work

In this paper we will use Convolutional Neural Networks (CNN), which are a common type of DL methods very effective for image classification. The first successful CNN was presented in [8] and it was designed for hand-written digit recognition. This early CNN implementation used a combination of convolution, pooling and non-linearity that has been the key feature of DL since now. The DL breakthrough took place with the publication of [9], where for the first time a CNN won the Imagenet[10] classification competition by a large margin. In that paper a set of innovative techniques were introduced including data augmentation, the use of rectified linear units (ReLUs) as activation function, the use of dropout for avoiding overfitting, overlapping max-pooling for avoiding the averaging effects of avg-pooling and the use of GPUs for speeding up the training time. Later on, different CNN improvements were also published. In [11], it was the first time that small 3x3 convolution filters were used and combined as a sequence of convolutions. In [12] the authors introduced residual

networks. This networks used a combination of 3x3 convolutional layers with a by-pass of the input every two layers that was summed up to the output. Such bypasses improved the gradient propagation through the network allowing the design of deeper networks and improving the classification capabilities.

DL models have also been successfully applied in many medical classification tasks. In [13] a DL classifier was designed achieving dermatologist-level accuracy for skin cancer detection. In [14] a 3D CNN for automated pulmonary nodule detection and classification was designed. In [15] a CNN Alzheimer's disease classifier with high performance was also described.

Many DL based DR classifiers have been published in the last years. In [16] a review of the different fundus photography based deep learning models for diagnosis of diabetic retinopathy is presented. In [17] the authors propose a novel disease-staging system for grading diabetic retinopathy that involves a retinal area not typically visualized on fundoscopy and another method that directly suggests treatments and determines prognoses. In [18] the authors propose a multiple instance learning method for DR detection, which jointly learns features and classifiers from data and achieves a significant improvement on detecting DR images and their inside lesions. In [19], they use an adaptive kernel visualization technique to produce DR image feature maps. Such maps are able to identify lesions causing the disease. Remarkable performance has been achieved with a deep learning model was published for the distinction of the most severe cases of DR [20]. It was trained using an extended version of the EyePACS dataset, improving the tagging of each image by a voting mechanism between different ophthalmologists for deciding the tag of each image and by increasing the number of images of the original dataset, using in this case about 125,000 graded retina fundus images. This model surpassed the human expert capabilities, reaching at the final operating point approximately 97% sensitivity and 93.5% specificity. The main benefit of this model was the high specificity and sensitivity achieved for the prediction of the more severe cases of DR. However, it is a binary classifier. In [7], we proposed a DL interpretable classifier for the prediction of five different disease grades. EyePACS dataset was used for

training and the results were close to the obtained by trained ophthalmologists, reaching values of specificity and sensitivity greater than 90% and human-like accuracy in the detection of the 5 categories of the DR grading task. An interesting feature of this DL model is that it is hundreds of times smaller than the previous ones.

Deep learning models are very successful in the separation of elements in different classes, but they have a major concern, which is the difficulty of interpreting the reasons behind a particular classification. They are parameterized models with not less than tens of thousands of parameters. The interaction between them is very difficult to analyze, making unfeasible a direct interpretation. In last years different ways for result explanation of deep learning models have been developed. In [21] the authors use a propagation method for visualizing the results in pixel-space. In [22] a pixel-wise decomposition is used. The calculated scores are back propagated using a message passing technique allowing the score distribution through all the input pixels. In [23] proposed a technique called Class Activation Mapping (CAM) for identifying discriminative regions used by a restricted class of image classification CNNs which do not contain any fully-connected layers. In [24] a generalization of the CAM algorithm was proposed to make it applicable to a significantly broader range of CNN model families without requiring architectural changes or retraining any secondary learning component. In [7], we proposed a pixel-wise derived explanation model. The model is of general applicability and is able to generate explanations either at pixel level or at any network receptive field size.

3. Methods

In this section we first introduce the concepts that are needed for the definition of the new method of DL interpretation based on Independent Components Analysis (ICA). The new method proposed is explained and formalized in section 3.3. Finally, we explain the characteristics of the DL model for DR classification, which will be used to evaluate the method proposed.

3.1. The Quadratic Weighted Kappa index

In this work, we address an ordinal problem that consists on classifying an eye fundus image into 5 grades of the DR disease. Ordinal regression is a term used for multi-class classification for the cases where a underlying property can be used for pre-establishing an ordering of the classes. Several quality measures exist in the literature of machine learning and statistics for evaluating the qualify of an ordinal classification model [25]. Kappa is a well-known statistic coefficient defined by Cohen [26] to measure inter-rater agreement in such cases. Weighted Kappa [27] is another index used for measuring the goodness of a ordinal regression classification. In Weighted Kappa disagreements are penalized proportionally to a power of the distance between classes. The penalization most commonly used is the quadratic. In such cases, the index is commonly referred as Quadratic Weighted Kappa (referred as QWK or κ indistinctly in this paper).

In equation 1 we show the mathematical definition of QWK.

$$\kappa = 1 - \frac{\sum_{i,j} \omega_{i,j} O_{i,j}}{\sum_{i,j} \omega_{i,j} E_{i,j}} \quad (1)$$

, where:

C : is the number of classes

$i, j \in \{1, 2, \dots, C\}$

$O_{i,j}$: the number of observations classified in the i -th category by the prediction model and they are in the j -th category in the correct classification (i.e. "true value").

$E_{i,j}$: outer product between the two classification histogram vectors (prediction and "true value"), normalized such that E and O have the same sum.

$\omega_{i,j}$: weight penalization for every pair i, j . Generally, $\omega_{i,j} = \frac{(i-j)^n}{(C-1)^n}$. For linear penalization $n = 1$. For quadratic penalization (more commonly used and the studied in this paper): $n = 2$.

Examples of the usage of the κ index for measuring inter-rater agreement in the medical context are: the measure of reliability in scans interpretation [28], the evaluation of expert agreement in diagnosis of glaucoma [29], the evaluation of reliability of radiographic assessment [30], the inter-observer agreement evaluation in diabetic retinopathy detection [31], among many others.

3.2. Feature compression methods

Feature compression methods, based on dimensionality reduction techniques, allow the expression of the information present in high dimensional vectors into others that use less dimensions. Depending on the nature of the transformation applied, they can be classified into: linear methods [32] and non-linear ones [33]. Typical linear methods include Principal Components Analysis (PCA) [34], Singular Value Decomposition (SVD) [35], Linear Discriminant Analysis (LDA) [36] and Independent Component Analysis (ICA) [37]. Non-linear methods use a non-linear transformation for obtaining the compressed version of the vector space. Typical examples of algorithms of this category are kernel-based versions of the linear ones, like kernel-PCA [38], kernel-ICA [39], Multidimensional Scaling (MDS) [40], random projections [41], neural networks derived methods [42], t-SNE [43] and Uniform Manifold Approximation (UMAP) [44] between many others.

Principal Component Analysis (PCA) [34] is a linear compression technique that allows the extraction of the most important characteristics from data. The components obtained are sorted by the percentage of the variance explained. This type of transformation allows not only the identification of the number of components required for explaining a predefined percentage of the variance, but also the percentage of variance explained by each one of the individual components.

Independent Component Analysis (ICA)[37] is a statistical method for the separation of a multi-dimensional random signal into a linear combination of components that are statistically as independent from each other as possible. The theoretical foundation of ICA is based on the Central Limit Theorem, which

establishes that the distribution of the sum (average or linear combination) of N independent random variables approaches a Gaussian as $N \rightarrow \infty$. When ICA method is applied, it is assumed that such separation exist, ie. that is possible to express the signal as a linear combination of independent components (IC). Perfect independence between random variables is achieved when mutual information between them is zero. Mutual information can be expressed as the Kullback-Leibler divergence between the joint distribution and the product of the distributions of each variable. Mutual information can be decomposed, under linear transforms, as the sum of two terms: one term expressing the correlation of the components and one expressing their non-Gaussianity [45]. ICA uses optimization to calculate its components. Two types of optimization objectives can be used: minimize the mutual information or maximize the non-gaussianess of each component.

Being both PCA and ICA linear methods, the difference between them relies in the way the data projection is done. PCA looks for basis vectors that best explain the variance of your data, being orthogonal between each other. ICA sacrifices orthogonality in favor of minimizing mutual information, i.e. maximizing probabilistic independence. In PCA, components are sorted by importance, i.e. percentage of variance explained. In ICA, neither the vectors are sorted by order of importance nor it gives information about the percentage of information explained, requiring an external evaluation for fixing the optimal number of components.

3.3. Method proposed: ICA based interpretation procedure

In this paper we go a step forward in the interpretation of score maps. Instead of generating directly the pixel maps associated with a particular class, we try to identify and separate independent elements associated with the disease. Our new contribution comes from the identification, separation and visualization of the IC that explain a particular classification decision. We hypothesize that in order to achieve high performance classification scores, the network has to encode the information required to make the classification. Human experts

base its decisions in the number and types of lesions present in the image. That's why in some way, such information has to be present in a disentangled form in last layer feature space, previous to the output layer. Instead of directly visualizing the more important pixels under a classification decision, we split the information of such last feature layer into independent features using a Independent Component Analysis (ICA). A posteriori we use a pixel-wise relevance propagation derived method to visualize such independent component in input space. In this way, we can, not only generate importance pixel maps, but also differentiate between the underlying independent causes of the disease.

We focus on the last layer feature space, previous to the output layer linear combination, in order to identify its properties and try to isolate the independent elements that are determining the class to which the image is assigned. We apply ICA [37] using different number of components to identify the minimum of them required to achieve a classification score close enough to the achieved without such a dimensional reduction. ICA allows to find a linear representation of non-Gaussian data so that the components are statistically independent, or as independent as possible. Such a representation seems to capture the essential structure of the data in many applications, including feature extraction [37]. When the data is not Gaussian, there are higher order statistics beyond variance that are not being taken into account by the PCA technique. While PCA captures only uncorrelated components, these uncorrelated components are not necessarily independent for general distributions. ICA minimizes the mutual information (or relative Kullback-Leibler divergence) of non-Gaussian data because two distributions with zero mutual information are statistically independent [46].

After the training of the DL model, we apply ICA to the last layer feature space vectors, for calculating the optimal ICA transformational matrix. Using different number of IC and comparing the classification performance of the original model with the obtained using a linear combination of the reduced number of calculated components, it is possible to find the optimal number of components (n) that does not significantly reduce the classification performance of the

original model. We modify the original model adding a new layer after the last layer feature space to calculate online the components of every analyzed image. The calculated matrix is embeded in the trained network as a new layer (see fig. 1). The final classification is achieved linearly combining the low dimensional IC layer.

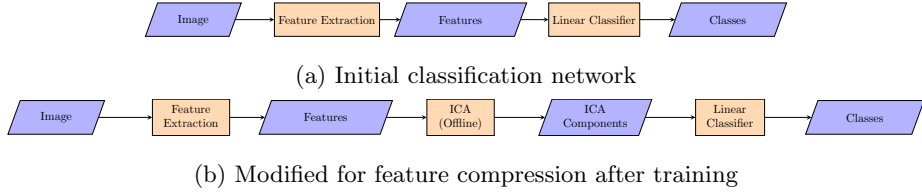


Figure 1: Model changes done for compressing feature-space

After identifying the optimal n , we use the receptive field and pixel-wise explanation model [7] to visualize the independent scores in the input space. In this way we are visualizing not only a score map explaining a classification but also differentiating and visualizing the mathematically IC responsible of a particular classification.

3.3.1. Mathematical formalization

Let F_{train} be the set of all feature vectors of training set:

$$F_{train} = \{\mathbf{f}^{(i)} : i = 1..T\}, \quad \mathbf{f}^{(i)} = (f_1^{(i)}, f_2^{(i)}, \dots, f_m^{(i)}) \quad (2)$$

being T the number of elements of the training set, and m the dimension of feature space vector.

Let S_{train} the set of IC calculated from F_{train} :

$$S_{train} = \{\mathbf{s}^{(i)} : i = 1..T\}, \quad \mathbf{s}^{(i)} = (s_1^{(i)}, s_2^{(i)}, \dots, s_n^{(i)}) \quad (3)$$

being n the number of IC, $n < m$.

Every $\mathbf{s}^{(i)}$ can be expressed as a linear combination of $\mathbf{f}^{(i)}$:

$$\mathbf{s}^{(i)} = \mathbf{W} \mathbf{f}^{(i)} \quad (4)$$

Where \mathbf{W} is calculated using a optimization method, minimizing the mutual information between n IC ($\min_S I(S)$) [47].

The ordinal regression problem solved using F_{train} can be expressed as:

$$\max_{\mathbf{A}} [\kappa_{val}(C_{train})] \quad (5)$$

being:

$$C_{train} = \{\mathbf{Af}^{(i)}, \forall f^{(i)} \in F_{train}\} \quad (6)$$

being $\mathbf{c}^{(i)} = \mathbf{Af}^{(i)}$ the predicted class vector and κ_{val} the evaluation function used in the training process of the neural network calculated for the validation set.

We want to solve the same problem using the reduced ICA components (feature space compressed version):

$$C'_{train} = \{\mathbf{Bs}^{(i)}, \forall s^{(i)} \in S_{train}\} \quad (7)$$

being $\mathbf{c}'^{(i)} = \mathbf{Bs}^{(i)}$ the predicted class vector using n IC.

The optimal number of IC to select is the one that minimizes the difference in performance between both models:

$$\min_n [\kappa_{val}(C'_{train}) - \kappa_{val}(C_{train})] \quad (8)$$

3.4. Baseline DL model for DR grading

We use as base of our study the deep learning model presented in [7]. It is a CNN of 17 layers and 391,325 parameters, that expect to receive RGB images of 640x640 pixels of resolution with black background and trimmed borders. Model layers are divided in two groups: the feature extractor and the classifier. The feature extraction has 7 blocks of 2 layers. Every layer is a stack of a 3x3 convolution with stride 1x1 and padding 1x1 followed by a batch normalization and a ReLU activation function. Between every block a 2x2 max-pooling operation of stride 2x2 is applied. The classifier is a 2x2 convolution. Finally, a

4x4 average-pooling is used for getting a final 64 feature vector that is linearly combined for obtaining the output scores of every class. The feature extractor has 16 filters in the first block, 32 in the second and 64 in all the others.

4. Results

4.1. Data

In this paper we use the EyePACS dataset. For every patient right and left eye images are present. All images are classified by ophthalmologists according to the standard severity scale presented before in [48]. From the 88,650 images of the dataset, 10,000 are used for testing purposes, 3,000 for validation and 75,650 for training. They are chosen by patient random selection, ie. left and right eye images of each patient must be present in the same set. Due to random selection, class frequency in all sets is expected to be the same. In table 1 we show the data distribution of the dataset. It can be observed, that it is an unbalanced dataset that requires sampling techniques for balance it at training time.

C0	C1	C2	C3	C4
73.7%	7.0%	14.7%	2.6%	2.0%

Table 1: Class distibution percentages in EyePacs train and test datasets

4.2. Application of the ICA-based DL model for DR grading and interpretation

After training the DL network, we calculate the last layer feature space for the whole training set, obtaining a 64-dimensional vector as a representation of each image. Then we have to find the best ICAs using the 64-dimensional feature-space vectors ($m = 64$) in the last layer of the DL model (before the classification part). As the best number of ICAs is not known, different values of n are explored. With each one, we apply a linear classifier and calculate the QWK metric on a validation set (as depicted in the procedure illustrated in Fig.

	T0	T1	T2	T3	T4
P0	6544	306	185	7	5
P1	695	376	352	7	6
P2	92	46	554	39	12
P3	11	3	335	155	36
P4	21	0	35	12	166

Table 2: Test set confusion matrix of original model (T: tagged, P: predicted)

1b). We choose the minimal n that allows achieving maximum performance, following the procedure presented in section ???. The optimal n for this problem is 3, achieving a $QWK_{val} = 0.785 \pm 0.01$ (95% confidence) not far from the achieved by the original model without dimensionality reduction ($QWK_{val} = 0.805 \pm 0.01$ (95% confidence)). Figure 2 shows the original confusion matrix and Figure 3 the confusion matrix after applying ICA.

We have also calculated the sensitivity (SN), specificity (SP) and F_1 score for a binarized version of the DR problem (Classes 0, 1 vs Classes 2,3,4). The values for the original model, according to its confusion matrix are SN=0.705, SP=0.979, F_1 =0.785. The values for the ICA derived model are SN=0.810, SP=0.940 and F_1 =0.785. As we can see, although the operating point is not the same, F_1 score for both models remains unchanged. The presented confusion matrices are designed for maximizing QWK, that is why the chosen operating point is not optimal in the balancing sensitivity and specificity for 0, 1 vs 2,3,4 classification. It is not the purpose of this paper to use the network for solving such binary classification. In case willing to use it in that way, another more balanced operating point should be chosen.

Fig. 2 shows the contribution of each component to the score of each class. We can see that ICA values distinguish clearly three classes (0, 2 and 4) but not class 1 and class 3. The same can be observed in the ICA confusion matrix.

In this regard, it is important to note that Diabetic Retinopathy is an ordinal regression problem, where classes 1 and 3 are defined as intermediate transitions

	T0	T1	T2	T3	T4
P0	7121	491	347	10	6
P1	0	0	0	0	0
P2	207	236	859	67	23
P3	0	0	0	0	0
P4	35	4	255	143	196

Table 3: Test set confusion matrix of the ica derived model (T: tagged, P: predicted)

between the other classes. Thus, we can see that this automatic model maintains the quality of prediction in terms of the QWK index by just using the 3 most relevant classes, despite doctors are normally using the 5 categories.

As we are training the network using as a loss function QWK , the optimization takes place as an ordinal regression. We expect the network to find the underlying causes present in the image that produce the predefined sorting of the classes, ie. the types of lesions and the number of them. Class 0 score contributions come from $ICA_0 > 0$, $ICA_1 > 0$ and $ICA_2 > 0$; being the class markers of the presence of disease $ICA_0 < 0$, $ICA_1 < 0$ and $ICA_2 < 0$.

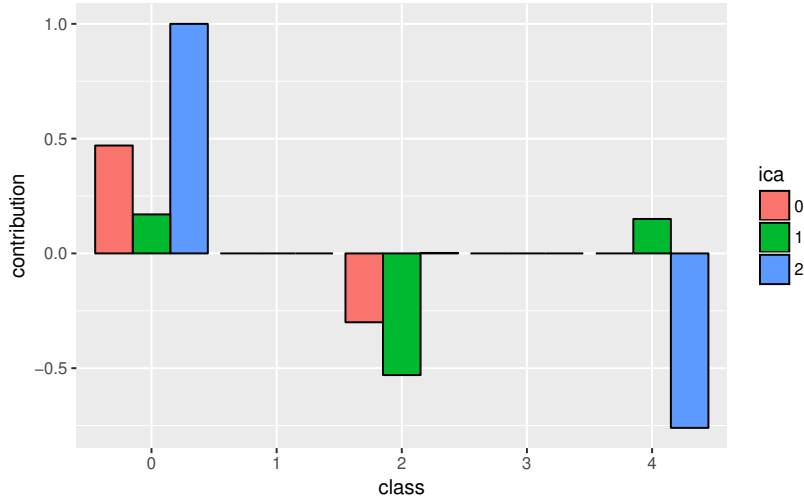


Figure 2: Weight of each ICA component in the classification final score (scaling=1e3)

We use a two-dimensional t-SNE visualization [43] for qualitative evaluation of the difference between the quality of the separation using the 64 feature vector and the reduced version with only 3 ICA components. In fig. 3 we show the 2D t-SNE visualization for the original feature space and for the ICA reduced space. We can see how for both spaces class 0, 2 and 4 classes are clearly separated. Class 0 and 1 are not properly separated and in the case of 3 and 4, although the separation is not perfect, it is possible to distinguish a different location of both classes for both spaces.

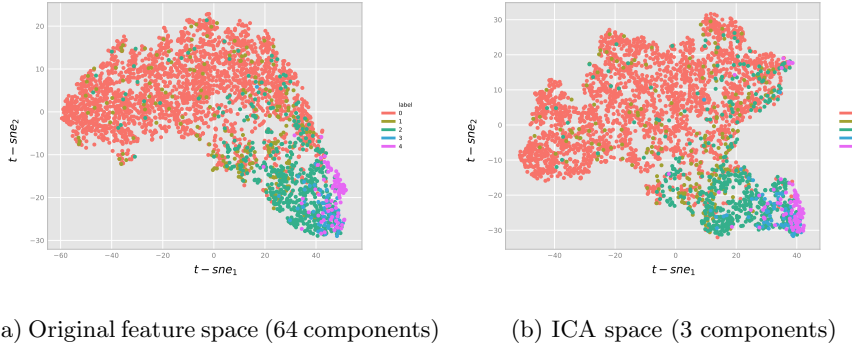


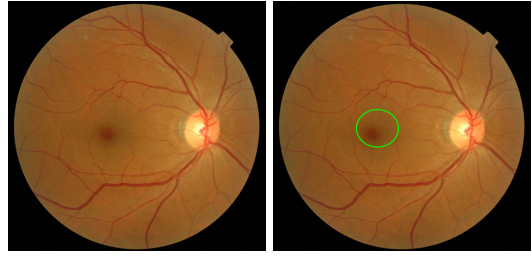
Figure 3: Comparison between the 2D t-SNE visualization of validation set using the original feature space and the final 3-dimensional ICA space

4.3. Score components contribution for different test samples

We apply a pixel-wise relevance propagation method to visualize each ICA component independently. In this way, it is possible to visualize the mathematically independent contributions of each axis and finding the localization of different types of primary elements causing the disease.

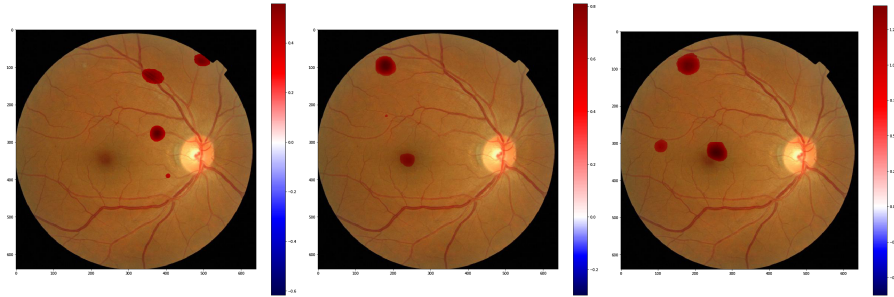
Figures 5, 7 and 9 show the intermediate score maps generated using a receptive field of 61x61. Figures 4, 6 and 8 show the original retinographies and the most important lesion zones identified by expert ophthalmologists prior to the generation of ICA lesion maps.

Figure 4 shows an example of a mild case of DR. We presented the results obtained from the model to an expert ophthalmologist in order to validate them.



(a) Original image (b) Real lesion zones

Figure 4: Class 1 image



(a) $ICA_0 < -3\sigma$ (b) $ICA_1 < -3\sigma$ (c) $ICA_2 < -3\sigma$

Figure 5: ICA explanation maps generated using a receptive field of 61x61

The expert concludes that all the regions identified by ICA_1 and ICA_2 correspond to real lesions. In the case of ICA_0 the expert identifies the top center zone as a false positive.



(a) Original image (b) Real lesion zones

Figure 6: Class 2 image

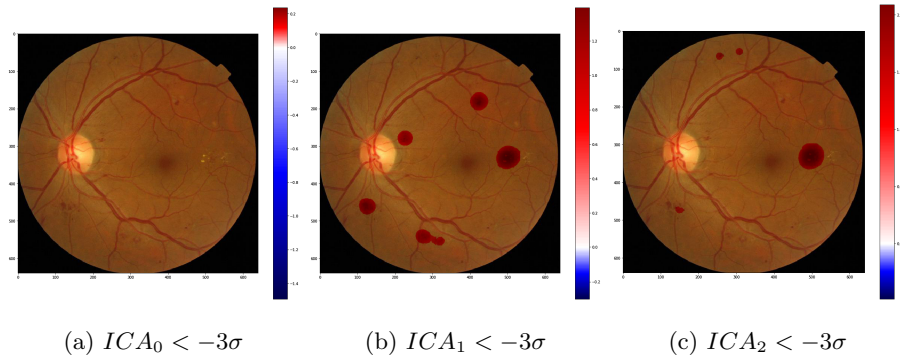


Figure 7: ICA explanation maps generated using a receptive field of 61x61

The same expert-based validation has been done with other images. Figure 6 shows an example of a moderate case of DR. The expert says that all the regions identified by ICA_1 and ICA_2 correspond to real lesions. In the case of ICA_0 in this case, no lesion zones are detected by the model.

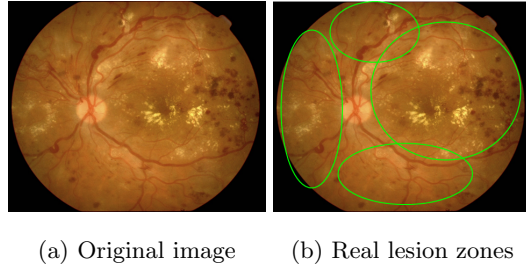


Figure 8: Class 4 image

Figure 8 corresponds to an example of a proliferative case of DR. The ophtalmologist indicates that all the regions identified by ICA_1 and ICA_2 correspond to real lesions. In the case of ICA_0 , the small lesion detected in the top of the image is also a real lesion. In this case, the nature of the lesion is different from the other but it is also caused by the diabetic retinopathy disease.

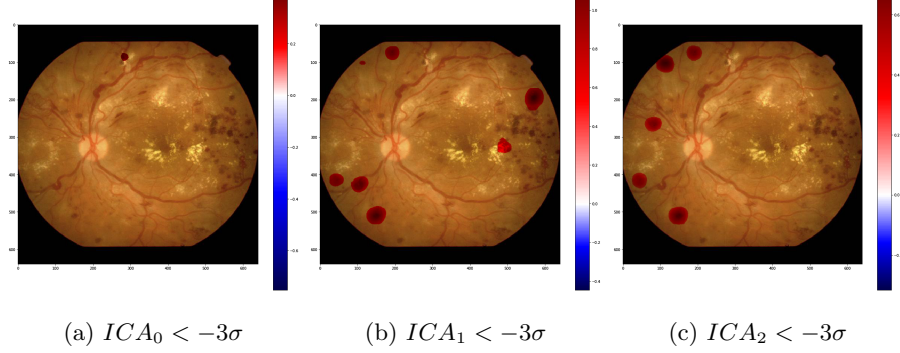


Figure 9: ICA explanation maps generated using a receptive field of 61x61

5. Discussion

With the compression technique presented in this paper and the use of a visualization technique, we can generate explanation maps as the ones shown in the previous section that are independent of the predicted class. This kind of maps provide a very valuable information to the ophthalmologists when they need to make a diagnosis of the degree of development of the DR disease. Some of the eye lesions are so small and the color is so similar to the eye background that its location and identification is really difficult for the person. However, if images are preprocessed with this method and some regions are marked, the person can pay attention to these parts of the image in order to verify if there are some lesions there.

The pixels with higher negative signals in the three components will give us the points that are contributing the most to the signaling of a possible presence of the disease. Backpropagating the scores of each one of these negative components will give evidences that help to the distinction of the signs of the final diagnostic given by the deep learning model.

An important point of the results obtained is that the QWK scores obtained with the initial model and the compressed one are really close. This shows that there is not a difference in the separation capability between the t-SNE map of the original features and the map of the ICA 3 dimensional compressed feature

map. The performance obtained for the original model was $\kappa_{orig} = 0.805$ and for the new one using ICA it is $\kappa_{ICA} = 0.790$, almost equivalent. In fact, it is not significant at 95% confidence. So, we can conclude that the independent component analysis has been able to find a adequate compressed expression of the information encoded in the network in a much reduced set of vectors. Thus, the method has been able to find independent vectors that are able to represent the classes of diabetic retinopathy from the information extracted from a deep learning model.

We have also compare the performance of ICA unsupervised compression with other linear compression techniques, like PCA. Using 3 PCA components, that explain 91% of the variance a $\kappa_{PCA} = 0.695$ is obtained. Far from the one obtained with ICA of 0.79.

It is worth to note that the visualization process of the information coming from these independent vectors in the original image can be done at different levels of generality, depending on the layer of the network. Hidden layer maps of figures 5, 7 and 9 are useful when a general map of the lesion locations is enough. Input-space pixel scores are the most suitable when pixel detail is required for detecting the individual lesions causing the disease.

The utility of such maps has been positively corroborated by some ophthalmologists, experts in DR diagnosis. Moreover, they have validated that score maps have an almost perfect match with real lesions having a very low rate of false positives and false negatives. It seems that, ICA_0 include sometimes some statistical regularities not directly related with relevant lesions. From such interpretation we conclude that ICA acts as a filter separating lesion information present in images from blink artifacts, noise and other statistical regularities present in images. Such artifacts are found mainly in ICA_0 .

6. Conclusions

In this paper, we studied some of the feature space properties of a already trained diabetic retinopathy deep learning classifier of 17 layers. We saw how,

even being a small network, the redundancy of the feature space is very high. We hypothesized that if the network is able to achieve human-level classifications, in some way, it has been able to identify the important statistical regularities present in the image that are important for the classification. As last layer is a linear classifier, such properties has to be disentangled, ie. expressed in a linear way in such last layer. We applied a independent component analysis over such last layer with the method explained in the paper in order to find the optimal number of components that maximize the classification capabilities of such compressed version of the features. We experimentally proved that reducing to only 3 components is possible to achieve almost 99% of the evaluation metric. Such value experimentally prove that the ICA compression has been able to extract all the important elements required for the classification. With such elements, we applied a visualization technique for identifying the elements in the image of each one of the components, using a pixel-wise derived visualization technique. We are able to generate three maps for every image each one identifying independent statistical regularities important for the classification.

Being able to find independent components is important to explore the possibility of using a machine learning method that builds a decision model that uses these vectors together with other patient's data to make a better diagnosis of the patient's risk of developing Diabetic Retinopathy. In fact, we have started to build such system using fuzzy random forests with information coming from the Electronic Health Record of diabetic patients [49, 50]. However, up to now, it is not possible to include the vectors obtained from the images because we do not have the eye fundus images of the patients of this database. A hospital in our region is now involved on collecting the appropriate data to make this study possible.

Finally, the method presented in this paper allows not only the classification of retinographies but also the identification and localization in the image of the mathematicaly independent features found by the classifier. The presented ICA score model is of general applicability and can be easily adapted for the usage in other image classification tasks thus, as future work we plan to test it in other

types medical images (eg. cancer detection in mammograms).

Acknowledgements

This work is supported by the URV grants 2018PFR-URV-B2-61 and 2017PFR-URV-B2-60, and the Spanish research projects PI18/00169 and PI15/01150 (Instituto de Salud Carlos III and Fondos FEDER). The authors would like to thank to Kaggle and EyePACS for providing the data used in this paper.

References

- [1] Pedro Romero-Aroca, Ramon Sagarra-Alamo, Marc Baget-Bernaldiz, Juan Fernández-Ballart, and Isabel Méndez-Marin. Prevalence and relationship between diabetic retinopathy and nephropathy, and its risk factors in the north-east of spain, a population-based study. *Ophthalmic epidemiology*, 17(4):251–265, 2010.
- [2] Pedro Romero-Aroca. Managing diabetic macular edema: The leading cause of diabetes blindness. *World journal of diabetes*, 2(6):98, 2011.
- [3] Yann Lecun, Yoshua Bengio, and Geoffrey Hinton. Deep learning. *Nature*, 521(7553):436–444, 5 2015.
- [4] J. Schmidhuber. Deep learning in neural networks: An overview. *Neural Networks*, 61:85–117, 2015.
- [5] Yoshua Bengio, Aaron Courville, and Pascal Vincent. Representation learning: A review and new perspectives. *IEEE Trans. Pattern Anal. Mach. Intell.*, 35(8):1798–1828, August 2013.
- [6] Yoshua Bengio. Learning deep architectures for AI. *Foundations and Trends in Machine Learning*, 2(1):1–127, 2009.
- [7] Jordi de la Torre, Aida Valls, and Domenec Puig. A deep learning interpretable classifier for diabetic retinopathy disease grading. *Neurocomputing*, 2019.

- [8] Y. LeCun, L. Bottou, Y. Bengio, and P. Haffner. Gradient-based learning applied to document recognition. *Proceedings of the IEEE*, 86(11):2278–2324, November 1998.
- [9] Alex Krizhevsky, Ilya Sutskever, and Geoffrey E Hinton. Imagenet classification with deep convolutional neural networks. In F. Pereira, C. J. C. Burges, L. Bottou, and K. Q. Weinberger, editors, *Advances in Neural Information Processing Systems 25*, pages 1097–1105. Curran Associates, Inc., 2012.
- [10] J. Deng, W. Dong, R. Socher, L.-J. Li, K. Li, and L. Fei-Fei. ImageNet: A Large-Scale Hierarchical Image Database. In *CVPR09*, 2009.
- [11] Karen Simonyan and Andrew Zisserman. Very deep convolutional networks for large-scale image recognition. *International Conference on Learning Representations, ICLR 2015*, 2015.
- [12] Kaiming He, Xiangyu Zhang, Shaoqing Ren, and Jian Sun. Deep residual learning for image recognition. In *Proceedings of the IEEE conference on computer vision and pattern recognition*, pages 770–778, 2016.
- [13] Andre Esteva, Brett Kuprel, Roberto A Novoa, Justin Ko, Susan M Swetter, Helen M Blau, and Sebastian Thrun. Dermatologist-level classification of skin cancer with deep neural networks. *Nature*, 542(7639):115, 2017.
- [14] Wentao Zhu, Chaochun Liu, Wei Fan, and Xiaohui Xie. Deeplung: Deep 3d dual path nets for automated pulmonary nodule detection and classification. In *IEEE Winter Conference on Applications of Computer Vision*, 2018.
- [15] Shui-Hua Wang, Preetha Phillips, Yuxiu Sui, Bin Liu, Ming Yang, and Hong Cheng. Classification of alzheimers disease based on eight-layer convolutional neural network with leaky rectified linear unit and max pooling. *Journal of medical systems*, 42(5):85, 2018.

- [16] Rajiv Raman, Sangeetha Srinivasan, Sunny Virmani, Sobha Sivaprasad, Chetan Rao, and Ramachandran Rajalakshmi. Fundus photograph-based deep learning algorithms in detecting diabetic retinopathy. *Eye*, page 1, 2018.
- [17] Hidenori Takahashi, Hironobu Tampo, Yusuke Arai, Yuji Inoue, and Hidetoshi Kawashima. Applying artificial intelligence to disease staging: Deep learning for improved staging of diabetic retinopathy. *PloS one*, 12(6):e0179790, 2017.
- [18] Lei Zhou, Yu Zhao, Jie Yang, Qi Yu, and Xun Xu. Deep multiple instance learning for automatic detection of diabetic retinopathy in retinal images. *IET Image Processing*, 12(4):563–571, 2017.
- [19] Stuart Keel, Jinrong Wu, Pei Ying Lee, Jane Scheetz, and Mingguang He. Visualizing deep learning models for the detection of referable diabetic retinopathy and glaucoma. *JAMA ophthalmology*, 137(3):288–292, 2019.
- [20] V. Gulshan, L. Peng, and M. Coram. Development and validation of a deep learning algorithm for detection of diabetic retinopathy in retinal fundus photographs. *Journal of the American Medical Association*, 316(22):2402–2410, 2016.
- [21] Matthew D Zeiler and Rob Fergus. Visualizing and understanding convolutional networks. In *European conference on computer vision*, pages 818–833. Springer, 2014.
- [22] Sebastian Bach, Alexander Binder, Grégoire Montavon, Frederick Klauschen, Klaus-Robert Müller, and Wojciech Samek. On pixel-wise explanations for non-linear classifier decisions by layer-wise relevance propagation. *PloS one*, 10(7):e0130140, 2015.
- [23] Bolei Zhou, Aditya Khosla, Agata Lapedriza, Aude Oliva, and Antonio Torralba. Learning deep features for discriminative localization. In *Proceedings*

of the IEEE conference on computer vision and pattern recognition, pages 2921–2929, 2016.

- [24] Ramprasaath R Selvaraju, Michael Cogswell, Abhishek Das, Ramakrishna Vedantam, Devi Parikh, and Dhruv Batra. Grad-cam: Visual explanations from deep networks via gradient-based localization. In *Proceedings of the IEEE International Conference on Computer Vision*, pages 618–626, 2017.
- [25] Nijat Mehdiyev, David Enke, Peter Fettke, and Peter Loos. Evaluating forecasting methods by considering different accuracy measures. *Procedia Computer Science*, 95:264–271, 2016.
- [26] Jacob Cohen. A coefficient of agreement for nominal scales. *Educational and psychological measurement*, 20(1):37–46, 1960.
- [27] Jacob Cohen. Weighted kappa: Nominal scale agreement provision for scaled disagreement or partial credit. *Psychological bulletin*, 70(4):213, 1968.
- [28] Susan R Hintz, Thomas Slovis, Dorothy Bulas, Krisa P Van Meurs, Rebecca Perritt, David K Stevenson, W Kenneth Poole, Abhik Das, Rosemary D Higgins, NICHD Neonatal Research Network, et al. Interobserver reliability and accuracy of cranial ultrasound scanning interpretation in premature infants. *The Journal of pediatrics*, 150(6):592–596, 2007.
- [29] Rohit Varma, William C Steinmann, and Ingrid U Scott. Expert agreement in evaluating the optic disc for glaucoma. *Ophthalmology*, 99(2):215–221, 1992.
- [30] Klaus P Günther and Yi Sun. Reliability of radiographic assessment in hip and knee osteoarthritis. *Osteoarthritis and Cartilage*, 7(2):239–246, 1999.
- [31] S Patra, EMW Gomm, M Macipe, and C Bailey. Interobserver agreement between primary graders and an expert grader in the bristol and weston diabetic retinopathy screening programme: a quality assurance audit. *Diabetic Medicine*, 26(8):820–823, 2009.

- [32] John P Cunningham and Zoubin Ghahramani. Linear dimensionality reduction: Survey, insights, and generalizations. *The Journal of Machine Learning Research*, 16(1):2859–2900, 2015.
- [33] Alireza Sarveniazi. An actual survey of dimensionality reduction. *American Journal of Computational Mathematics*, 4(02):55, 2014.
- [34] Ian Jolliffe. *Principal component analysis*. Springer, 2011.
- [35] Gene H Golub and Christian Reinsch. Singular value decomposition and least squares solutions. In *Linear Algebra*, pages 134–151. Springer, 1971.
- [36] Sebastian Mika, Gunnar Ratsch, Jason Weston, Bernhard Scholkopf, and Klaus-Robert Mullers. Fisher discriminant analysis with kernels. In *Neural networks for signal processing IX: Proceedings of the 1999 IEEE signal processing society workshop (cat. no. 98th8468)*, pages 41–48. Ieee, 1999.
- [37] Aapo Hyvärinen and Erkki Oja. Independent component analysis: algorithms and applications. *Neural networks*, 13(4-5):411–430, 2000.
- [38] Sebastian Mika, Bernhard Schölkopf, Alex J Smola, Klaus-Robert Müller, Matthias Scholz, and Gunnar Rätsch. Kernel pca and de-noising in feature spaces. In *Advances in neural information processing systems*, pages 536–542, 1999.
- [39] Jian Yang, Xiumei Gao, David Zhang, and Jing-yu Yang. Kernel ica: An alternative formulation and its application to face recognition. *Pattern Recognition*, 38(10):1784–1787, 2005.
- [40] Ingwer Borg and Patrick Groenen. Modern multidimensional scaling: Theory and applications. *Journal of Educational Measurement*, 40(3):277–280, 2003.
- [41] Dmitriy Fradkin and David Madigan. Experiments with random projections for machine learning. In *Proceedings of the ninth ACM SIGKDD*

international conference on Knowledge discovery and data mining, pages 517–522. ACM, 2003.

- [42] Geoffrey E Hinton and Ruslan R Salakhutdinov. Reducing the dimensionality of data with neural networks. *science*, 313(5786):504–507, 2006.
- [43] Laurens van der Maaten and Geoffrey Hinton. Visualizing data using t-sne. *Journal of machine learning research*, 9(Nov):2579–2605, 2008.
- [44] Leland McInnes, John Healy, Nathaniel Saul, and Lukas Großberger. UMAP: uniform manifold approximation and projection. *J. Open Source Software*, 3(29):861, 2018.
- [45] Jean-François Cardoso. Dependence, correlation and gaussianity in independent component analysis. *Journal of Machine Learning Research*, 4:1177–1203, 2003.
- [46] Pierre Comon. Independent component analysis, a new concept? *Signal processing*, 36(3):287–314, 1994.
- [47] Aapo Hyvärinen. Fast and robust fixed-point algorithms for independent component analysis. *IEEE transactions on Neural Networks*, 10(3):626–634, 1999.
- [48] CP Wilkinson, FL Ferris 3rd, Ronald E Klein, Paul P Lee, Carl David Agardh, Matthew Davis, Diana Dills, Anselm Kampik, R Pararajasegaram, and Juan T Verdaguer. Global diabetic retinopathy project group. proposed international clinical diabetic retinopathy and diabetic macular edema disease severity scales. *Ophthalmology*, 110(9):1677–1682, 2003.
- [49] Emran Saleh, Aïda Valls, Antonio Moreno, and Pedro Romero-Aroca. Integration of different fuzzy rule-induction methods to improve the classification of patients with diabetic retinopathy. In *Recent advances in Artificial Intelligence Research and Development, Frontiers in Artificial Intelligence and Applications*, volume 300, pages 6–15. IOS Press, 2017.

- [50] Emran Saleh, Jerzy Błaszczyński, Antonio Moreno, Aida Valls, Pedro Romero-Aroca, Sofia de la Riva-Fernández, and Roman Słowiński. Learning ensemble classifiers for diabetic retinopathy assessment. *Artificial intelligence in medicine*, 85:50–63, 2018.